JGR Planets

RESEARCH ARTICLE
10.1029/2019JE006197

Key Points:
- The long-term average ion environment at Phobos is constrained from 4 years of in situ measurements
- Planetary atomic and molecular oxygen ions dominate solar wind ions in sputtering the surface of Phobos downstream of Mars
- The flux of material sputtered from the surface of Phobos increased by a factor of 50 during the March 2015 solar wind events

Correspondence to:
Q. Nénon,
q.nenon@gmail.com

Citation:
Nénon, Q., Poppe, A. R., Rahmati, A., Lee, C. O., McFadden, J. P., & Fowler, C. M. (2019). Phobos surface sputtering as inferred from MAVEN ion observations. *Journal of Geophysical Research: Planets*, *124*, 3385–3401. https://doi.org/10.1029/2019JE006197

Received 4 SEP 2019
Accepted 27 NOV 2019
Accepted article online 11 DEC 2019
Published online 23 DEC 2019

Phobos Surface Sputtering as Inferred From MAVEN Ion Observations

Q. Nénon[1,2], A. R. Poppe[1,2], A. Rahmati[1], C. O. Lee[1], J. P. McFadden[1], and C. M. Fowler[1]

[1]Space Sciences Laboratory, University of California at Berkeley, Berkeley, CA, USA, [2]Solar System Exploration Research Virtual Institute, NASA Ames Research Center, Mountain View, CA, USA

Abstract Phobos is bombarded by both protons and alpha particles from the solar wind and by Martian atomic and molecular oxygen ions. A numerical model of the distribution of planetary ions has previously proposed that these ions may dominate solar wind ions in sputtering the surface of Phobos when the moon is located downstream of Mars. This conclusion suggests a unique link between planetary atmospheric escape at Mars and the surface processing of its moon yet, remains to be confirmed with in situ ion measurements. In this article, a 4-year-long average of the ion environment that Phobos is exposed to is constructed from in situ ion observations conducted by the Mars Atmosphere and Volatile Evolution (MAVEN) mission. In turn, the flux of material sputtered from the surface of Phobos by this environment is computed. We confirm that planetary atomic oxygen ions dominate over solar wind ions in sputtering the surface of Phobos downstream of Mars during 20% of the moon's orbit. We also reveal that molecular oxygen ions sputter the surface of Phobos as much as or more than atomic oxygen ions in the Martian magnetotail. In addition to the long-term average picture, the time variation of Phobos surface sputtered fluxes is investigated during the series of solar wind events that hit the Martian system in March 2015. We find that the flux of material liberated from Phobos' surface increased by a factor of 50 during this period.

Plain Language Summary Phobos is the closest of the two moons of Mars and its surface is bombarded by positively charged particles, ions, that liberate surface material into space (sputtering). The moons of Mars are exposed to not only ions coming from the solar wind but also to ions coming directly from the atmosphere of their host planet. Previous work used a numerical model to study the relative importance of solar wind and Martian ions in sputtering the surface of Phobos and found that ions coming from Mars may be important, in particular when Phobos is behind Mars with respect to the Sun. However, this has never been discussed or studied with in situ measurements of ions. In this article, we use observations of ions obtained by the NASA Mars Atmosphere and Volatile Evolution mission (MAVEN), in orbit around Mars since 2014, to confirm that ions coming from Mars dominate solar wind ions in sputtering the surface of Phobos in the nightside. We also find that the flux of material liberated from the moon surface can increase by a factor of 50 during solar wind events.

1. Introduction

Sputtering of airless body surfaces by ions is a universal process by which asteroids, comets, and satellite surface material is liberated and, depending on the local gravity, falls back onto the surface or is released into space. Phobos and Deimos, the two moons of Mars, are bombarded by ions that come from the Martian atmosphere and are hereafter named "planetary ions". If sputtering by planetary ions were important against sputtering by solar wind ions, then the Martian moons' surface evolution would be intimately coupled to their host planet atmospheric escape. This situation would be unique in the Solar System, as the Moon is negligibly affected by terrestrial ions (Poppe et al., 2018) and giant planet moons are altered by either the solar wind or magnetospheric plasma, neither of which is sourced by the host planet exosphere.

Ions that can impact Phobos have been observed in situ by three instruments onboard the 3-month long Phobos-2 mission (Barabash et al., 1991; Dubinin et al., 1993; Verigin et al., 1991), during more than 14 years by the ion instrument of the ASPERA-3 experiment onboard Mars Express (Ramstad et al., 2018, and

references therein), and have now been sampled for more than 4 years by three ion instruments onboard the Mars Atmosphere and Volatile Evolution (MAVEN) mission (Halekas et al., 2017; Inui et al., 2019; Jakosky et al., 2015; Lee et al., 2017).

All these observations have shown that the upstream solar wind plasma during quiet conditions is composed of mainly protons and 1% to 5% of alpha particles, has a typical density of 1–3 cm^{-3} and a typical bulk velocity of 350–450 km/s (Ramstad et al., 2017). The plasma slows and becomes denser and hotter downstream of the induced magnetospheric bow shock (Dubinin et al., 2006). Solar wind ions have a limited access to the magnetotail region, located downstream of Mars (see Liemohn & Xu, 2018, and references therein).

Solar energetic particle (SEP) events add suprathermal particles with kinetic energies up to several MeV to the previous typical solar wind ions. A survey of SEP ion events observed by MAVEN has been established by Lee et al. (2017), but the average high energy tail spectra that Phobos is exposed to over several years has never been constrained. Poppe et al. (2018) constructed this high-energy tail for the Moon with ARTEMIS ion observations and pointed out its importance in creating amorphous rims on lunar dust grains (e.g.,Christoffersen et al., 1996 ; Keller & McKay, 1997).

Phobos-2, Mars Express, and MAVEN have shown that planetary ions at the orbit of Phobos are mainly protons, O^+ ions, $O_2{}^+$ ions, and in a lower extent, $CO_2{}^+$ ions. These ions come from two sources, the first one being directly the Martian ionosphere, as ions escape through the polar plume and Martian plasma wake (Dong et al., 2015; Dong et al., 2017; Dubinin et al., 1993; Inui et al., 2019; Verigin et al., 1991). Neutral particles from the Martian exosphere or neutral corona, which is large enough to extend upstream of the Martian bow shock, are the second seed population for planetary ions, created when neutral particles are ionized and then picked up and accelerated by the background electromagnetic environment, reaching energies higher than several tens of keV (Barabash et al., 1991; Rahmati et al., 2015, 2017, 2018).

Typical plasma parameters of the upstream solar wind can be used to compute a first estimate of the solar wind induced sputtering and enabled Cipriani et al. (2011) to show that ions are expected to liberate orders of magnitude more surface material than micrometeoroid bombardment at Phobos. However, typical solar wind parameters are not sufficient to discuss the importance of energetic ions brought by transient SEP events nor the role that planetary ions may play. Regarding planetary ions, existing surveys do not give differential energy fluxes but only fluxes and moments integrated over large energy ranges (Dubinin et al., 2006; Inui et al., 2019; Lundin et al., 2013). These parameters are not sufficient to estimate Phobos surface sputtering due to planetary ions that have energies as low as a few eV and as high as several tens of keV. In the absence of a survey of energy differential flux of planetary ions, the relative importance of solar wind and planetary ions in Phobos surface sputtering can only been inferred by using numerical models of planetary ion distributions, like the ones published by Modolo et al. (2005), Curry et al. (2014), or Farrell et al. (2018). The only existing model-based effort to discuss the importance of solar wind and planetary ions in Phobos surface sputtering has been conducted by Poppe and Curry (2014), who pointed out that oxygen planetary ions dominate the solar wind induced sputtering in regions downstream of Mars. However, this has never been discussed or confirmed with in situ measurements.

In this article, we use MAVEN in situ ion observations to constrain the solar wind and planetary ion population distributions at Phobos' orbit and discuss their importance in Phobos surface sputtering. Section 2 of the paper shows how the orbit of MAVEN and its three ion instruments enable a heretofore unprecedented ability to conduct this effort. Section 3 shows the long-term average ion environment that Phobos is exposed to based on more than 4 years of MAVEN in situ measurements. This environment is composed of three populations: the typical solar wind, the high energy tail brought by SEP events, and Martian planetary ions. The flux of material sputtered by these three long-term average populations is computed in section 4, where the relative importance of each ion population is discussed in the different plasma regions encountered by Phobos (solar wind, magnetosheath, and magnetotail). In addition to the long-term average picture, the time variability of Phobos sputtered fluxes is investigated during the well-documented March 2015 series of interplanetary coronal mass ejections and associated SEP events in section 5. Finally, section 6 summarizes our findings and their implications.

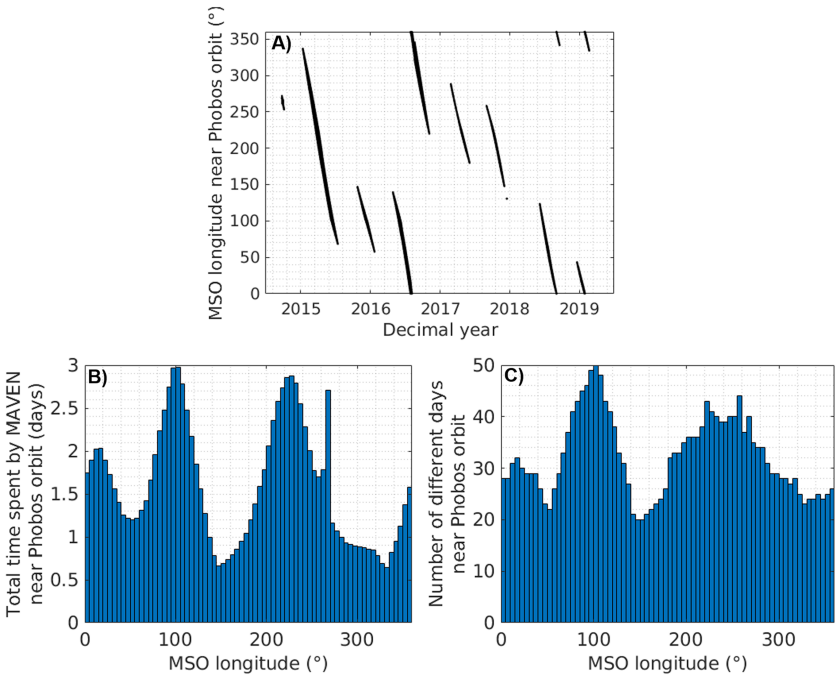

Figure 1. (a) MSO longitudes crossed by MAVEN when the spacecraft was at distances to the center of Mars greater than 9,000 km and had an MSO latitude between −27° and +27° (specified by, near Phobos orbit). Each MSO longitude is observed during 2 to 4 time intervals distributed over the mission duration. (b) Time spent by MAVEN in 5° wide MSO longitude bins near Phobos orbit for the entire mission. (c) Number of different days when MAVEN was near the orbit of Phobos in 5° wide MSO longitude bins.

2. Data and Method: Phobos and MAVEN Orbits and MAVEN Ion Measurements

2.1. Phobos and MAVEN Orbits

In this study, we use the Mars-Solar-Orbital (MSO) coordinate system. It is Mars centered, the *X* axis points from Mars to the Sun, the *Y* axis is antiparallel to the Mars orbital velocity, and the *Z* axis completes the right-handed coordinate system. Phobos completes a revolution around Mars in 7.6 hours along an orbit that has a periapsis (minimum distance to the center of Mars) of 9,234 km, an apoapsis of 9,518 km and an inclination of around 1° with respect to the Martian equatorial plane. Since the Mars equatorial plane is inclined by 26° with respect to the ecliptic plane, Phobos traverses MSO latitudes between −27° and +27°.

MAVEN entered into orbit around Mars on 21 September 2014. After a 2-month commissioning phase, the primary science mission started on 16 November 2014 (Jakosky, Grebowsky, Luhmann, & Brain, 2015). Since then and up to February 2019, the apoapsis of MAVEN has been at around 9,590 km. (For comparison, Phobos is between 9,234 and 9,518 km.) For each MAVEN orbit, observations conducted in situ near apoapsis may therefore directly sample the environment that Phobos is exposed to.

In order to constrain the ion environment at the orbit of Phobos, we aggregate observations obtained by MAVEN at distances greater than 9,000 km and MSO latitudes between −27 and +27°. This region is called in this paper the “orbit of Phobos”. However, sampling of this region by MAVEN is complicated by two orbital constraints. First, MAVEN's apoapsis does not always lie in the latitude range of interest (−27° to +27°). Secondly, for times when the apoapsis is within applicable latitudes, MAVEN observes only a few MSO longitude degrees at each Phobos orbit crossing. Figure 1a shows the MSO longitudes crossed by MAVEN near the orbit of Phobos as a function of time. It can be seen that the orbit latitude precession causes the spacecraft to cross the latitudes of interest near apoapsis during most of the mission (note that blank periods in the figure show when it did not). The first useful observations after the commissioning phase were gathered on 9 January 2015 for MSO longitudes around 340°. After this date, MAVEN crossed the orbit of Phobos at various MSO longitudes as a result of the MSO coordinate frame rotation together with MAVEN's longitudinal

precession. It can be seen in Figure 1a that MAVEN observed each MSO longitude during 2 to 4 different periods that are distributed along the mission duration, in its first and second half. More solar wind events have been observed during the first half of the mission (i.e., in 2015 and 2016), than in the second half (2017–2019) (Lee et al., 2017), so that the mission-averaged measurements compiled in section 3 capture quiet and active periods at each MSO longitude.

MAVEN spent between 0 and 50 minutes in the region of interest during each 4.5-hour orbit, for a total integrated time spent near Phobos orbit of 115 days. The distribution of this total time according to MSO longitude is shown in Figure 1b in 5° wide bins. MAVEN spent a factor of 3 to 4 more time at MSO longitudes around 0°, 100°, and 220° than at MSO longitudes around 150° and 330°. In order to construct an average ion environment representative of what is seen by Phobos in section 3.3, we will therefore average measurements obtained in each longitude bin separately rather than average all measurements together, in order to not give more weight to the most observed regions.

The time spent by MAVEN within a given 5° longitude window ranges from 0.5 to 3 days, but observations obtained within each longitude window were actually gathered on different days. Figure 1c shows the number of unique days during which observations were collected within each longitude window. This ranges from 20 to 50, and these days are, as shown by Figure 1a, distributed in different periods of the mission.

MAVEN in situ measurements can therefore be used to construct, for the first time, a long-term average picture of the ion environment seen by Phobos at all MSO longitudes that represent different plasma regions around Mars: the solar wind, the magnetosheath, and the magnetotail. In addition, observations gathered over several days or weeks can be used to study the time dynamics of the ion environment (see section 5), even if only in a limited longitude range at a time (Figure 1a).

2.2. MAVEN Ion Instruments

2.2.1. The Three Instruments SEP, SWIA, and STATIC Observe Together the Full Ion Kinetic Energy Range

MAVEN is not only uniquely positioned to constrain the ion environment that Phobos is exposed to, it is also fully equipped to observe ions with three instruments that we describe below: SEP, SWIA and STATIC.

2.2.1.1. SEP

The MAVEN Solar Energetic Particle experiment, SEP, consists of two double-ended sensors (named SEP1 and SEP2) comprised of a triple silicon layer detector stack that measures 20 keV to >6 MeV ions. Each sensor has two look directions: the "Forward" look direction (SEP1F and SEP2F), which is nominally pointed in the Parker spiral interplanetary magnetic field direction, and the "Reverse" look direction (SEP1R and SEP2R), which is 180° away from the forward direction (Larson et al., 2015).

We use in this study Level 2 data that are accumulated over 1, 2, 8, or 32 seconds, depending on the spacecraft altitude and Earth-Mars downlink rates. The top panel of Figure 2 shows an energy time spectrogram of the differential ion energy flux (ion flux multiplied by the ion kinetic energy) observed by SEP 2F on 5 and 6 April 2016. During this period, some hydrogen or oxygen pickup ions are observed (the discrete fluxes in the ~20 to 30-keV range), such as at 02:00 UT on April 6 (Rahmati et al., 2015, 2017, 2018). No energetic particle fluxes linked to solar wind events were observed, which typically have energy fluxes greater than 100 eV/(eV.cm^2.s.sr) at energies higher than 100 keV (Lee et al., 2017).

The background created by Galactic Cosmic Ray particles (GCRs) and solar X-ray can be seen in the top panel of Figure 2 (Larson et al., 2015). In order to estimate and remove this background, a time period with no planetary pickup ions or energetic events at all had to be found. The background is estimated from observations obtained during 14 and 15 November 2018. This background has been found to not affect the long-term average of MAVEN/SEP energy fluxes presented in section 3.3, even when multiplying it by a factor of 2. It means that the signal coming from energetic particles, even if brought by transient events, is strong enough to overcome the MAVEN/SEP instrument noise level due to Galactic Cosmic Rays particles and solar X-rays on a long-term basis.

When the attenuator of a MAVEN/SEP telescope is closed, the effective background level is increased by a factor of 100 because of the reduction in the MAVEN/SEP geometric factor, as seen in Figure 2 (top panel) on

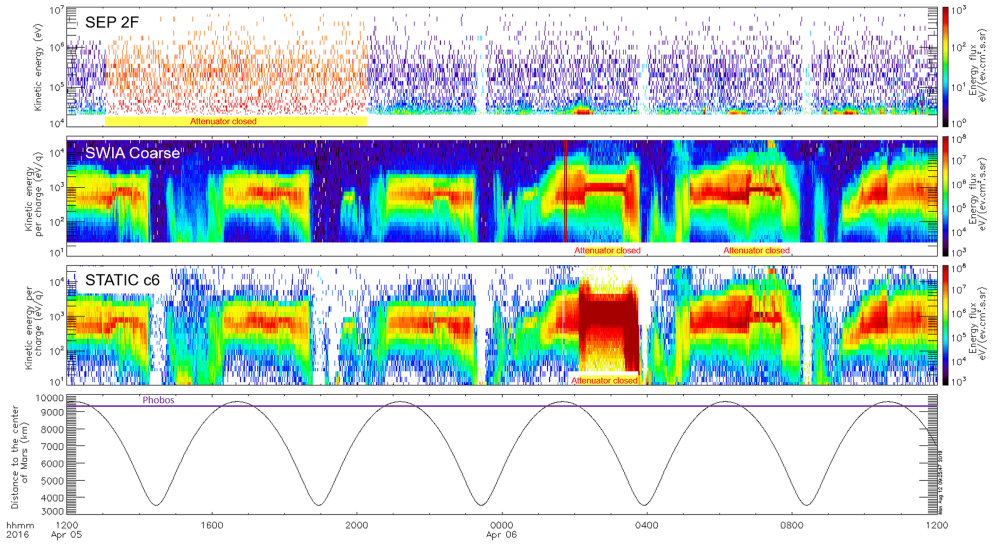

Figure 2. Energy-time spectrogram of ion energy fluxes observed by SEP 2F (first panel), SWIA (second panel), and STATIC (third panel). The last panel gives the distance of MAVEN to the center of Mars and the horizontal purple line shows the distances of the orbit of Phobos. The yellow areas show when a mechanical attenuator of SEP, SWIA, or STATIC is closed.

5 April between 13:00 and 20:00. During these closed attenuator periods, the background level is high enough so that we exclude these periods.

Finally, it is worth noting that the particle kinetic energies shown here and retrieved from Level 2 files assume that all observed particles are protons in order to estimate energy losses through the instrument and convert deposited energy to incident energy. However, oxygen ions lose on average 50 keV more than protons before impacting the detectors (Rahmati et al., 2015), so that if the ions observed with an energy of 20 keV for instance are oxygen ions and not protons, their incident energy would be around 70 keV, not 20 keV (see discussion in section 3.3).

2.2.1.2. SWIA

The MAVEN Solar Wind Ion Analyzer (SWIA) is a toroidal electrostatic analyzer that observes ions with kinetic energy per charge of 25 eV/q to 25 keV/q (Halekas et al., 2015). It is not able to identify ion species. The main objective of SWIA is to observe the solar wind, and two data products are produced every 4 seconds: "Coarse", which gives observations from the full field-of-view of the instrument, and "Fine", which focuses on the limited portion of the sky where the solar wind comes from (see Figure 9 of Halekas et al., 2015). We look in this study for the omnidirectional flux that impacts Phobos, so that we use SWIA "Coarse" data.

The sources of background in SWIA measurements are discussed in Halekas et al. (2015) and Halekas et al. (2017). In Figure 2, second panel, the background is seen to create energy fluxes between 10^4 and 10^5 eV/(eV.cm^2.s.sr). Although the background slightly increases when the mechanical attenuator closes, it remains sufficiently low so that measurements obtained with the closed configuration are kept in this study. The background increases by a factor of around 5 during solar energetic events (not shown on Figure 2). In order to account for the time varying background, we estimated it by visually inspecting energy-time spectrograms day by day. This inspection also enables us to remove artifacts, such as the two vertical red lines seen on 6 April around 01:45 UT.

2.2.1.3. STATIC

The MAVEN SupraThermal And Thermal Ion Composition instrument (STATIC) is a toroidal electrostatic analyzer that observes ions with kinetic energy per charge from 0.1 eV/q to 30 keV/q (McFadden et al., 2015). A unique capability of the instrument is that it accelerates selected ions with a −15 kV potential and measures their time of flight (TOF) through a chamber. The TOF capacity of STATIC enables the instrument to identify ion masses with a resolution of $\frac{\Delta M}{M} \approx 25\%$. STATIC measurements are recorded in different data products with varying resolutions in energy, mass, and angular coverage, and possess different

acquisition rates. In this study, we use the "c6" product, which gives every 4 seconds a measurement of ion fluxes averaged over the whole field-of-view of the instrument (see section 2.2.2) binned in 32 energy channels and 64 mass channels.

Sources of uncertainties and background are discussed in McFadden et al. (2015). STATIC has a lower background than SWIA thanks to the TOF coincidence, as can be seen in Figure 2, third panel. We correct STATIC observations for coincident events that are produced by two different particles creating a start and stop signal, following McFadden et al. (2015) (see in particular their equations 5 and 6 page 237). We also remove low mass shoulder fluxes produced by molecular O_2^+ and CO_2^+ ions (see Figures 33 and 34 of McFadden et al., 2015). The two previous backgrounds are estimated for "c6" observations by using together other STATIC data products that have the same acquisition cadence of 4 seconds but add to the "c6" product more information on valid, start, and stop event rates ("d8", "da") have better energy resolution ("c0") or keep track of the distribution of counts with respect to anodes and deflection angles ("c8", "ca"). When available, similar or lower cadence products are also used: "d8", "d9", and "db". For the definition of the STATIC data products, we refer the reader to the Software Interface Specification document published in the MAVEN STATIC Planetary Data System repository (see acknowledgments section).

The ability of STATIC to distinguish ion species is powerful and appealing, as it enables us to determine the multispecie ion environment of Phobos and to study separately protons, alpha particles, atomic oxygen and molecular oxygen ions. However, a known unresolved problem of STATIC in mass identification is the presence of proton and alpha particle "stragglers". Stragglers have the same energy as solar wind ions but are identified to have higher masses because they remain in the TOF chamber for longer than expected. This creates a high-mass tail, as seen for instance in Figure 17 of McFadden et al. (2015). Stragglers are therefore a source of background for alpha particles, atomic oxygen, and molecular oxygen ion measurements. There is currently no software to effectively remove the straggling induced background, but section 4 shows that this does not impact our conclusions regarding Phobos surface sputtering.

STATIC uses an electrostatic and a mechanical attenuator to increase its dynamical range by a factor of 1,000. The mechanical attenuator only closes half of the field of view of STATIC and because of STATIC's ability to point using the MAVEN Articulated Payload Platform, the attenuator is sometimes closed yet the solar wind enters the instrument in an uncovered sector. The result of that can be seen on Figure 2 from 02:00 to 04:00 on 6 April, with very high and unrealistic fluxes. We therefore do not use measurements obtained by STATIC when the mechanical attenuator is closed. Finally, it is worth noting that the measurements used in this study are not corrected for ion acceleration by the spacecraft surface potential, but this does not affect our conclusions (see section 3.1).

2.2.2. MAVEN Ion Instruments Fields of View, Looking for the Omnidirectional Flux

In order to study the surface sputtering of Phobos, we are interested by the omnidirectional ion flux. However, MAVEN is a three-axis stabilized spacecraft (i.e., is not spinning), so that measurements averaged over the field of view of each instrument may not be entirely representative of omnidirectional ion fluxes.

The two electrostatic analyzers, SWIA and STATIC, have distributed anodes to observe all directions within a plane (360°) and use electrostatic deflectors to reach elevation angles of ±45° for energy per charge lower than ~5 keV/q. They therefore each observe 70% of the sky. Above 5 keV/q, the elevation angle coverage reduces with increasing energy due to high voltage constraints and reaches a minimum elevation of ±7° at 30 keV (Halekas et al., 2015; McFadden et al., 2015; Rahmati et al., 2017), thereby observing only 12% of the whole sky. The STATIC FOV can sometimes partly be blocked by the spacecraft body, as a result of its pointing being governed by the Articulated Payload Platform. Each of the four MAVEN/SEP fields of view is a rectangle spanning 31° by 42°, observing around 3% of the whole sky (Larson et al., 2015). Together, the four SEP look directions therefore observe around 12% of the whole sky.

Two assumptions can be made in order to estimate omnidirectional fluxes from FOV averaged observations. The first one is to consider that an instrument catches the full ion distribution within its FOV, so that fluxes outside of the FOV are equal to 0. This is the most conservative approach and enables one to set a lower boundary on the omnidirectional flux. In that case, the omnidirectional flux is equal to the instrument FOV-averaged flux multiplied by the observed fraction of the sky (0.7 for SWIA and STATIC below 5 keV/q and 0.12 for SEP). A second possibility is to assume that the flux observed over the FOV is representative of the omnidirectional flux. It is exactly true if the flux is isotropic, like for >100 keV ions (see section 3.2).

In this study, we assume that fluxes observed by each instrument are representative of the omnidirectional ion flux that impact Phobos (i.e., the second assumption from above). This assumption is further discussed in section 3.2, in particular when FOV-averaged fluxes are compared from one instrument to another.

3. The Long-Term Average Ion Environment That Impacts the Surface of Phobos

3.1. Multispecie Ion Observations by STATIC

Figure 3 shows in 5° wide MSO longitude bins the MAVEN mission long-term average differential energy flux of protons, alpha particles, atomic oxygen ions, and molecular oxygen ions observed by the STATIC instrument. Other ion species, like for instance CO_2^+, are found with STATIC measurements to have fluxes low enough compared to the previous four species to negligibly sputter the surface of Phobos.

Above each panel of Figure 3, the top colored line shows the position of the Martian bow shock given by Trotignon et al. (2006) that separates the "solar wind" region (red line) from the "magnetosheath" region (yellow line). The region with MSO longitudes between 135° and 225° is labeled as the "magnetotail" (blue line), to describe the region where solar wind ion fluxes are seen to be significantly reduced compared to upstream conditions and where cold plasma ion fluxes are enhanced. This "magnetotail" region, as we call it hereafter, actually encloses regions named by Nagy et al. (2004) as the magnetic pileup region and the plasma sheet. The actual shape of the magnetotail is very complex and dynamic and cannot be delimited with simply an MSO longitude range (Liemohn & Xu, 2018).

3.1.1. STATIC Solar Wind and Higher Energies

In the solar wind and magnetosheath, the solar wind protons are seen to have kinetic energies between 400 eV and 2 keV, while alpha particles have energies per charge twice that of the protons, around 800 eV/q to 4 keV/q. This is consistent with protons and alpha particles having velocities close to the solar wind bulk velocity.

Proton stragglers, one of the known caveats of the STATIC instrument (see section 2.2), have energy per charge similar to protons but have longer time of flights and are therefore registered as if they have higher masses. These stragglers with energies around 600 eV are clearly seen in atomic oxygen and molecular oxygen ion measurements to be the source of artifact fluxes of around 10^4 eV/(eV.cm^2.s.sr) in the solar wind and magnetosheath regions. The stragglers are also likely to be the origin of 400 to 600 eV alpha particle fluxes with energy fluxes of 10^5 to 10^6 eV/(eV.cm^2.s.sr). As discussed in section 2.2, we cannot so far correct for the stragglers induced background, but section 4 will show that their presence in the data does not affect our conclusions on Phobos surface sputtering.

Oxygen ions are found at high kinetic energies at all MSO longitudes and are not negligible upstream of Mars. The energy-longitude topology of atomic oxygen ion fluxes observed in situ by STATIC is consistent with atomic oxygen ion distributions simulated by Poppe and Curry (2014) (see their Figure 1). Molecular oxygen ions are negligible compared to the three other species in front of Mars, for MSO longitudes between 0 and 50° and between 310 and 360°. Significant energy fluxes of O_2^+ ions appear in the magnetosheath at high kinetic energies, from 1 keV to 30 keV. Previous simulation studies correctly predicted the existence of this energetic population (see Figure 4 of Curry et al., 2014) but have shown that O_2^+ fluxes are at least an order of magnitude lower than O^+ fluxes. Using MAVEN STATIC measurements, Inui et al. (2018, 2019) have shown that molecular oxygen ion fluxes actually dominate over atomic oxygen ion fluxes at cold plasma energies. To the best of our knowledge, our study reports for the first time that this is also true at high kinetic energies, from 1 to 30 keV, as energetic O_2^+ fluxes are seen on Figure 3 to be similar to O^+ fluxes in the sheath region. This side product of our study may provide new constraints on Martian atomic and molecular oxygen atmospheric escape.

We have checked that >1 keV O^+ and O_2^+ ion fluxes in the sheath are not proton stragglers by using the 64 mass bins of the STATIC "c6" product to produce energy-mass plots similar to Figure 37 of McFadden et al. (2015). Proton stragglers should affect all the mass bins and create a monoenergetic "line" (vertical line on Figure 37 of McFadden et al., 2015) that we do not see for >1 keV O^+ and O_2^+ ions in the sheath.

3.1.1.1. STATIC Low Energies

One can see on Figure 3 that for energies lower than 500 eV in the solar wind and sheath regions, fluxes are dominated by protons that may originate either from the extended hydrogen corona of Mars (Rahmati et al.,

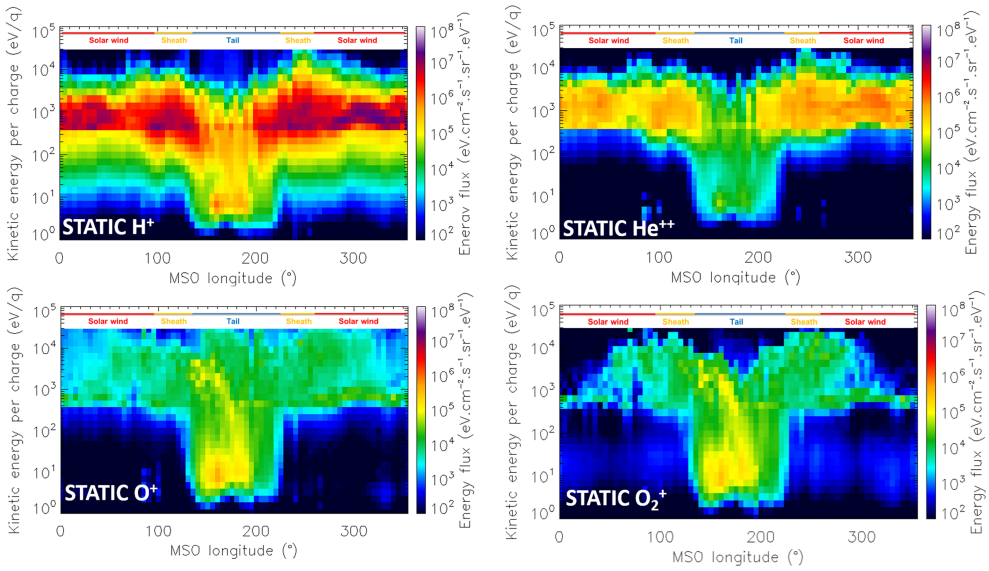

Figure 3. Long-term average differential proton, alpha particles, atomic oxygen, and molecular oxygen ion fluxes observed by STATIC near the orbit of Phobos along MSO longitude.

2017, 2018) or may be solar wind protons reflected from the bow shock and traveling away from Mars (Yamauchi et al., 2011). Relatively large fluxes of low energy protons, alpha particles, atomic oxygen, and molecular oxygen ions appear at energies of around 4 to 7 eV in the magnetotail. These cold ions are discussed in detail by Inui et al. (2019) and are likely to have energies lower than what is shown here, as we do not correct for acceleration by the spacecraft negative surface potential. However, only ions with kinetic energies higher than 80 eV significantly sputter the surface of Phobos (see section 4), so that the spacecraft negative surface potential does not impact the conclusions of this study. Finally, we note that cold and energetic oxygen ions in the tail region are not symmetric around the MSO longitude of 180° but are shifted toward lower longitudes, as expected from the simulations of Poppe and Curry (2014) (see their Figures 1a and 1b).

3.2. Comparison Between STATIC and SWIA

Figure 4 shows in 5° wide MSO longitude bins the long-term average differential energy flux of all ions observed by STATIC (left panel) and SWIA (right panel), assuming that the fluxes averaged over each instrument FOV are omnidirectional (see section 2.2.2). Having two instruments observing the kinetic energy range from 30 eV to 30 keV enables a unique cross comparison.

The agreement between the gross features seen in SWIA and STATIC ion observations is, overall, very good. The first most notable discrepancy between the two instruments can be seen in the solar wind at MSO

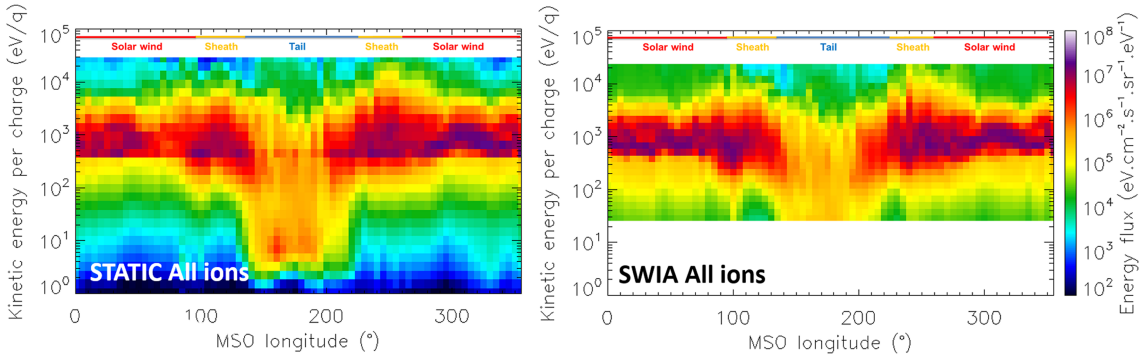

Figure 4. Long-term average differential total ion fluxes observed by STATIC and SWIA near the orbit of Phobos along MSO longitude.

longitudes around 70° at energies of around 600 eV. Indeed, SWIA observes ion energy fluxes consistent with other longitudes in the solar wind and magnetosheath regions (purple color), whereas STATIC observes a flux reduced by a factor of 3 to 5 (red color). This difference comes from the different orientations of STATIC and SWIA, even if both instruments observe 70% of the whole sky at this energy. Indeed, we find that at the altitude of Phobos, STATIC was pointed away from the solar wind more often at longitudes of 70° than at others. We therefore compute the flux of material sputtered from the surface of Phobos using both SWIA and STATIC inputs in section 4 to reach conclusions independent of the instrument pointing issue.

Different pointing between SWIA and STATIC also explains the fact that SWIA observes higher fluxes than STATIC in the solar wind region at energies higher than 10 keV, for which the instruments FOVs are relatively narrow (see section 2.2.2). Indeed, as discussed by Rahmati et al. (2017), the pointing of SWIA makes the instrument more likely to observe energetic pickup ions than STATIC.

3.3. Longitude Average Ion Kinetic Energy Spectra

3.3.1. STATIC Identifies the Dominant Ion Species

Figure 5a shows the kinetic energy spectra of protons, alpha particles, atomic oxygen, and molecular oxygen ions observed by STATIC at the orbit of Phobos during the whole MAVEN mission and averaged over all MSO longitudes. This is the average ion environment that Phobos is exposed to when orbiting around Mars.

The peak at low energies, around 6 eV, is not real but likely comes from cold ion acceleration by the spacecraft negative potential. A side product of this study is to point out that the surface potential near the STATIC instrument is on average between −4 and −8 V in the magnetotail.

The flux maximum is found at energies around 600 eV and is dominated by protons, consistent with a solar wind origin. Alpha particles dominate ion fluxes from 3 to 30 keV and have a maximum at 4 times the proton peak energy, consistent with protons and alpha particles having the same velocity. The ratio of the peak energy flux of alpha particles to the peak energy flux of protons is found by STATIC to be on average of 2.9%. Above 30 keV, STATIC observations suggest that planetary oxygen ions may dominate the total ion flux at Phobos.

Atomic oxygen and molecular oxygen ions have very similar kinetic energy spectra up to 8 keV, where molecular ion fluxes begin to drop. This feature comes from the fact that very energetic molecular oxygen ions (>~10 keV) are found for a more limited range of MSO longitudes, only in the magnetosheath region, than for oxygen ions, as shown by Figure 3. We have also checked that the MSO longitude average fluxes shown here are not affected by proton stragglers, in particular for energies around 600 eV where the proton flux is the highest. More than 80% of the longitude average atomic and molecular oxygen ion fluxes at this energy come from the flux enhancement seen in the tail on Figure 3 and are therefore not overly contaminated by straggling protons in the solar wind.

3.3.2. STATIC, SWIA, and SEP Together Define the Full Kinetic Energy Range

Figure 5b shows the time and MSO longitude average total ion fluxes observed by STATIC, SWIA, and MAVEN/SEP versus kinetic energy per charge (not kinetic energy as Figure 5a) for STATIC and SWIA, and versus kinetic energy for MAVEN/SEP.

SWIA and STATIC are in very good agreement, with a peak in energy flux at an energy per charge of around 600–700 eV. At 20 keV/q, the discrepancy between STATIC and SWIA reported and explained in section 3.2 is seen, with the average energy flux observed by SWIA being ~4 times higher than the average STATIC flux.

At even higher kinetic energies, the SEP 1F and SEP 2F look directions observe kinetic energy spectra that are very similar and would overlap if plotted on Figure 5b, so that only one curve is plotted. The same is true for SEP 1R and SEP 2R. For energies between 20 and 100 keV, the forward and reverse observations show a discrepancy of a factor of ~10. This is due to the fact that the front directions observe hydrogen and oxygen pickup ions originating from the Martian neutral corona that are not observed by the reverse directions (Rahmati et al., 2015). The omnidirectional flux at these energies is therefore best described as the average of the front and reverse MAVEN/SEP observations. At 20 keV, MAVEN/SEP flux measurements are around a factor of 3 to 5 lower than STATIC observations. However, energies shown for the MAVEN/SEP ions are retrieved from available Level 2 data files, which assume that the ion composition is dominated by protons. STATIC measurements tend to show that ion energy fluxes at 20 keV/q may instead be dominated by oxygen ions (see Figure 5a), so that these ions are likely to actually have an energy of around 70 keV, as discussed in

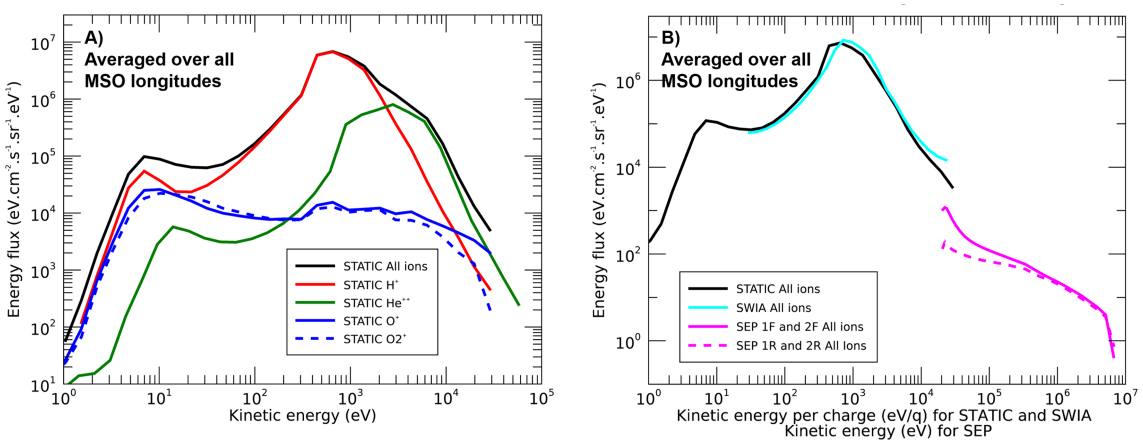

Figure 5. (a) MSO longitude and long-term average energy fluxes observed by STATIC near the orbit of Phobos. (b) The same for total ions observed by STATIC, SWIA, and SEP. The abscissa gives the kinetic energy per charge of observed ions for the STATIC and SWIA curves and the kinetic energy for the SEP curve.

section 2.2.1. In this case, the SEP 1F and 2F curves would therefore be shifted to the right of the figure for the lowest energy channels, so that there would not seem to be any spectral slope break from STATIC to MAVEN/SEP measurements. Given that we ultimately cannot determine the ion species measured by MAVEN/SEP, we have left the MAVEN/SEP curves as-is using the assumption that the measurements are due to incident protons.

Above ~300 keV, the four MAVEN/SEP look directions show the same average flux, which most likely originates from solar energetic particle events (Lee et al., 2017). This flux is therefore very likely representative of the omnidirectional flux. We show in this study for the first time the long-term average ion kinetic energy spectra due to transient solar energetic particle events at Mars. It is a similar effort to what has been done recently for the Moon with ARTEMIS observations by Poppe et al. (2018).

4. Flux of Atoms Sputtered From the Surface of Phobos by the Long-Term Average Ion Environment

The flux of atoms sputtered from the surface of Phobos by the long-term average ion environment presented in section 3 can now be computed. To do so, we assume that Phobos is small enough to be considered as a point bombarded by the ambient omnidirectional flux of ions, as assumed by Cipriani et al. (2011) and Poppe and Curry (2014). This assumption enables us to easily compute the flux of sputtered material from the whole surface of the moon, although we do not account for the local topology of Phobos and/or possible plasma wake development (Farrell et al., 2018).

The total flux of material sputtered from the surface of Phobos is computed with equation (1), as done by Poppe and Curry (2014), by convolving the flux of bombarding ions, written hereafter $J(E_k)$, with the energy dependent total sputtering yield $Y(E_k)$, which gives the mean number of sputtered neutral atoms per incident ion.

$$Sputtered\ flux\ \left[cm^{-2}.s^{-1}\right] = \int_{E_k} J\left(E_k\right)\left[cm^{-2}.s^{-1}.eV^{-1}\right].Y(E_k)[no\ unit]\ dE_k\ [eV] \tag{1}$$

The total sputtering yield $Y(E_k)$ is not only a strong function of the ion kinetic energy E_k (see for instance Figure 1c of Poppe & Curry, 2014) but also depends on the target composition. We only look here for the total sputtering yield and do not try to estimate target specie-discriminated yields, as the composition of the surface of Phobos is unknown (Pieters et al., 2014).

The determination of sputtering yields of ions with monoatomic and complex material is an active area of research, and most available estimates rely on Monte Carlo simulations conducted with either the SRIM/TRIM (Ziegler et al., 2008) or SDTrimSP (Mutzke et al., 2019) softwares, as experimental databases

keep growing but remain limited (Schaible et al., 2017; Szabo et al., 2018, and references therein). In this article, we use the total sputtering yields for impacting H^+, He^{2+}, and O^+ ions given by Figure 1 c of Poppe and Curry (2014), computed by Biersack and Eckstein (1984) for a monoatomic Ni target and very similar to estimates of Matsunami et al. (1984) for Ni or Fe atoms. Using these sputtering yields will enable us to easily compare our conclusions, based on ion fluxes determined from MAVEN observations, with the model-based conclusions of Poppe and Curry (2014).

One can compare the total sputtering yield used here with values published for complex material to get an idea of the uncertainty on computed sputtered fluxes introduced by using sputtering yields of monoatomic Ni or Fe surface. Barghouty et al. (2011) studied sputtering of KREEP material that can be found on the Moon (acronym for high concentration in potassium K, Rare Earth Elements, and Phosphorus) by impacting H^+, He^{2+}, and $O^{6+\ -8+}$ ions but only for a kinetic energy of 1 keV/amu. They found a sputtering yield of 0.024 for 1 keV/amu H^+ (we use in this work 0.015), 0.15 for 1 keV/amu He^{2+} (0.14 in this study), and 1.55 for 1 keV/amu $O^{6\ +\ -8+}$ (we use 1.3 for O^+ ions). At this specific kinetic energy, one can see that the sputtering yields that we use are in agreement with KREEP sputtering yield estimates of Barghouty et al. (2011) within less than a factor of 2. Schaible et al. (2017) computed energy-dependent sputtering yields of H^+ and He^{2+} on SiO_2 and Al_2O_3 targets. As for KREEP, the sputtering yields that we use here are within a factor of 2 in agreement with the yields published by Schaible et al. (2017).

Based on existing literature, an uncertainty of roughly a factor of 2 in the sputtering yields may exist, which would lead to an error of a factor of 2 in computed sputtered fluxes. We will show later in this section that such uncertainty does not affect our conclusions regarding the relative importance of Martian and solar wind ions in sputtering the surface of Phobos.

The sputtering yield of molecular oxygen ions, O_2^+, is computed from the sputtering yield of atomic oxygen ions, O^+, by assuming that the molecular ions breaks down when impacting the surface into two O^+ ions having each half of the initial kinetic energy of the O_2^+ ion. The sputtering yield of an O_2^+ ion with kinetic energy E_k is therefore taken to be twice the sputtering yield of an O^+ ion with kinetic energy $E_k/2$. This assumption has been shown by Steinbrüchel (1985) to be valid for at least Au and Si targets. Following Poppe and Curry (2014), the computed sputtered fluxes are finally multiplied by a factor of 0.71 to account for the likely surface porosity of Phobos.

Figure 6a shows the flux of neutral atoms sputtered from the surface of Phobos by the protons and alpha particles observed by the STATIC instrument (blue line) as a function of Phobos' MSO longitude. The peak energy flux ratio of alpha particles to protons of 2.9% observed by STATIC has been used to compute sputtered flux due to the solar wind as observed by SWIA (red line). The difference between the SWIA and STATIC observations of the solar wind at MSO longitudes around 70°, discussed previously in section 3.2, is found to create here a discrepancy of a factor of ~4 in the calculated sputtered fluxes. One can see on Figure 6a that the flux of sputtered atoms is predominantly produced by the solar wind while Phobos is in the solar wind and magnetosheath regions. Local increases of 50%–100% in the sputtered flux can be seen in the magnetosheath, where the flux of shocked solar wind deviating around Mars is increased over the upstream solar wind flux. In the magnetotail, MAVEN in situ measurements confirm that planetary atomic oxygen ions dominate the solar wind in sputtering the surface of Phobos as predicted by Poppe and Curry (2014). Indeed, in the tail region, the flux of material sputtered by oxygen ions is a factor of 10 higher than the sputtered flux due to protons and alpha particles, whereas the uncertainty in sputtering yields is of around a factor 2 (see previous paragraph).

Absolute values of sputtered fluxes computed here can be compared with the model-based results of Poppe and Curry (2014): The flux of neutral particles sputtered by solar wind ions in the solar wind region is of around 4–7 $\times$ 10^6 cm^{-2} s^{-1}, what is consistent with the value of 4 $\times$ 10^6 cm^{-2} s^{-1} used by Poppe and Curry (2014). In the magnetotail region, the sputtered flux due to O^+ ions observed by the STATIC instrument peaks at 2 $\times$ 10^6 cm^{-2} s^{-1}, what agrees within a factor of 2 with the simulation results of Poppe and Curry (2014) when the Interplanetary Magnetic Field (IMF) is taken to be representative of a typical Parker Spiral configuration. It means that the model of Poppe and Curry (2014), with Parker Spiral IMF configuration, captures the long-term average sputtered flux due to O^+ ions.

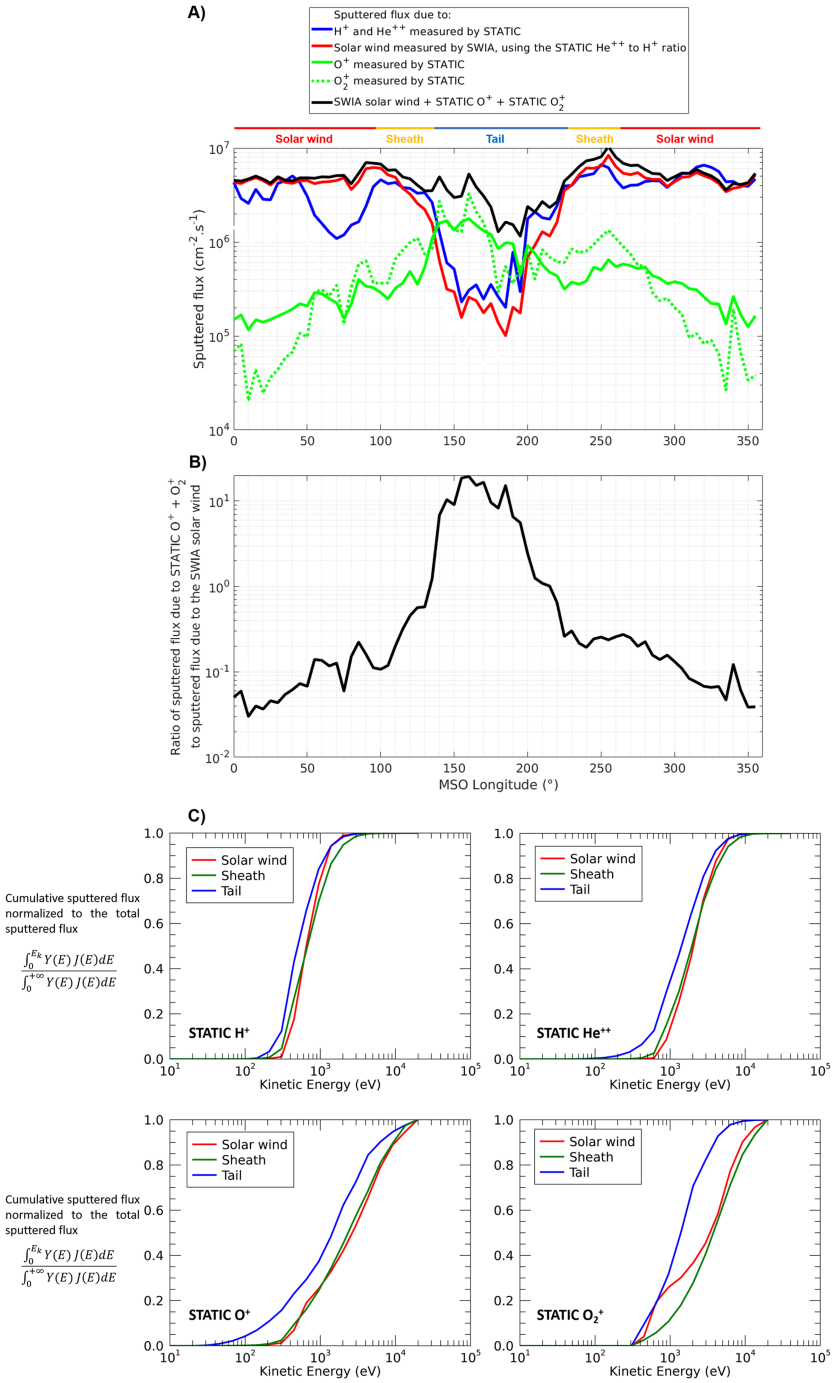

Figure 6. (a) Flux of material sputtered from the surface of Phobos by the ions observed by STATIC and SWIA along MSO longitude. Sputtering yields given by Poppe and Curry (2014) are used, and all sputtered fluxes are multiplied by 0.71 to account for the surface porosity (see main text). (b) Ratio of the sputtered flux created by planetary atomic and molecular oxygen ions to the sputtered flux due to the solar wind as a function of MSO longitude. (c) Cumulative sputtered flux due to protons, alpha particles, atomic oxygen and molecular oxygen ions observed by STATIC in the solar wind, magnetosheath, and magnetotail regions, normalized by the region-averaged total sputtered flux and given as a function of ion kinetic energy.

Energetic molecular oxygen ion fluxes were predicted to be at least an order of magnitude lower than oxygen ion fluxes before the MAVEN era (e.g., Curry et al., 2014; Poppe & Curry, 2014); however, section 3 of our study has shown that they have fluxes similar to O^+ ions, in particular in the magnetotail. MAVEN in situ

measurements therefore consequently reveal that molecular oxygen ions sputter the surface of Phobos as much or more than atomic oxygen ions in the tail region, as seen on Figure 6a (solid green line and dashed green line).

Figure 6b gives the ratio of sputtered flux due to planetary O^+ and O_2^+ ions to the flux sputtered by the solar wind protons and alphas. Planetary ions are found to dominate over the solar wind for MSO longitudes between 135° and 210° or during 20% of the orbit of Phobos. This clearly demonstrates that the escape of the Martian atmosphere via ion loss is a fundamental process in understanding the evolution of Phobos' surface downstream of the planet.

In Figure 6c, the sputtered flux computed from STATIC ion observations is averaged in each of the three regions: solar wind, magnetosheath, and magnetotail. We then compute the cumulative distribution by taking the integral between $E = 0$ and the abscissa kinetic energy of sputtered fluxes in each region and normalize the computed integral to the region-averaged total sputtered flux, which can be used to demonstrate which ion energies predominantly sputter the surface of Phobos in each of the three regions. We can see that, as expected, sputtering by solar wind ions is attributed to a narrow range of energy in the solar wind region as 90% of the flux of material liberated by protons (taking the normalized cumulative sputtered flux between 0.05 and 0.95) is attributed to 350-1,500 eV protons. The distribution of sputtered flux with solar wind ion energies broadens slightly in the magnetosheath region and shifts toward lower energies in the magnetotail region. Contrary to solar wind ions, sputtering by Martian oxygen ions comes from a relatively large range of energies, as for instance 90% of atomic oxygen-induced sputtered flux is due to O^+ ions with energies between 80 eV and 10 keV. We also note that the contribution to sputtering from molecular oxygen ions, O_2^+, comes from larger energies than atomic oxygen ions. Finally, Figure 6c can be used to estimate the impact of the proton straggler background (see section 3.1) on oxygen ion-induced sputtered fluxes. As stragglers are predominantly in the solar wind and magnetosheath regions and have energies lower than 1,000 eV (see section 3.1), we can conclude from Figure 6c that proton stragglers contribute to less than 25% of the total sputtered flux due to atomic and molecular oxygen ions. We note that the solar wind region shown in Figure 6c contains the region delimited by MSO longitudes between 310° and 40°, and that in this region, O_2^+ ion fluxes are completely dominated by proton stragglers (see Figure 3 and section 3.1).

Finally, we estimated the sputtered flux due to ions with energies above 20 keV observed by MAVEN/SEP using sputtering yields of either protons, alpha particles or oxygen ions, as the dominant ion specie is not known with certainty (see section 3.1). Even when using the highest sputtering yields (i.e., the ones of oxygen ions), we find that ions with energies above 20 keV contribute to less than 1% of the long-term total sputtered flux.

5. Time Variation of Phobos Sputtered Fluxes During the March 2015 Solar Wind Event

In addition to the long-term average picture presented in sections 3 (ion flux) and 4 (sputtered flux), MAVEN in situ measurements offer the opportunity to investigate how the sputtered fluxes change over time, even if only within a limited range of MSO longitudes at a time because of the MAVEN orbit (see Figure 1a).

A series of three to four Interplanetary Coronal Mass Ejections (ICMEs) impacted Mars from 25 February 2015 to 13 March 2015 (Jakosky, Grebowsky, Luhmann, & Brain, 2015; Lee et al., 2017). The subsequent reaction of ions in the Martian system to this event has been reported and discussed by Jakosky, Grebowsky, Luhmann, & Brain (2015) Jakosky et al. (2015), Curry et al. (2015), and Dong et al. (2015). Phobos orbits within this system and the evolution of the flux sputtered from its surface is investigated for the first time here. During this period, MAVEN crossed MSO longitudes near the orbit of Phobos between 269° (on 20 February) and 230° (on 13 March).

Figure 7 shows ion spectra observed by MAVEN/SEP 1F (top panel) and SWIA (second panel) during this period. STATIC observations, not shown on the figure, show that planetary atomic and molecular oxygen ions negligibly sputter the surface of Phobos at the MSO longitudes and times of interest (e.g., see Figure 6b). For the solar wind measurements, SWIA and STATIC measurements are in excellent agreement during this period.

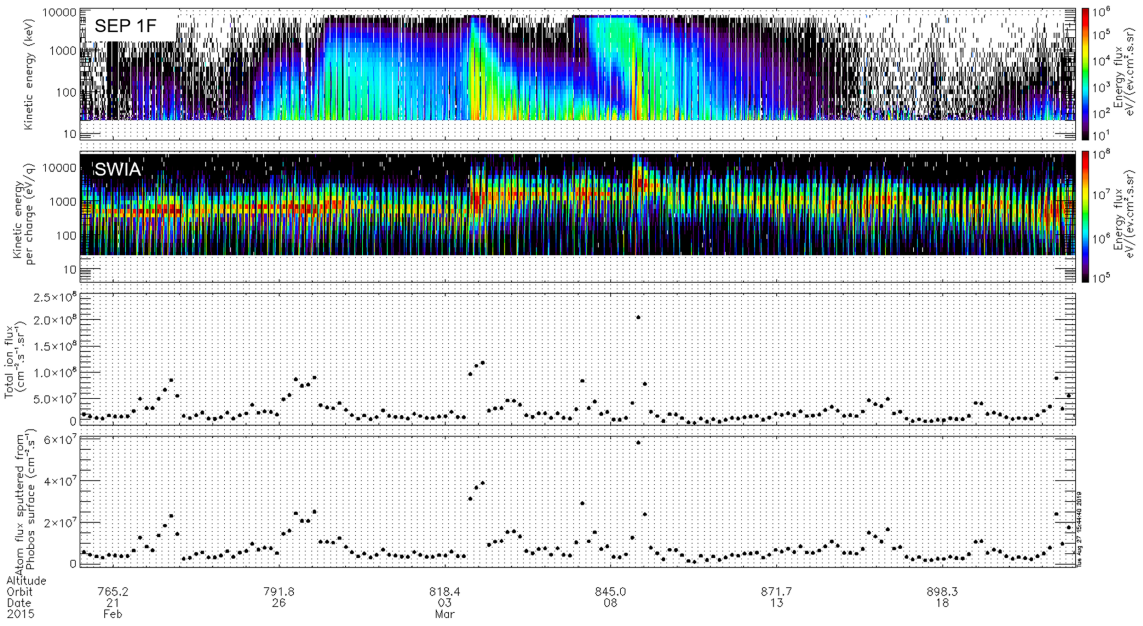

Figure 7. Energy-time spectrogram of ion differential energy flux observed by SEP 1F (first panel) and SWIA (second panel). The third panel gives the total ion flux, integrated over kinetic energy. MAVEN crossed MSO longitudes between 230° and 269° during the time period shown. The last panel gives the flux of material sputtered from the surface of Phobos for each MAVEN orbit, computed at each MAVEN apoapsis. Dotted vertical lines show periapsis passes.

In order to compute the flux of material sputtered from the surface of Phobos as a function of time, we average STATIC and SWIA ion spectra at each MAVEN apoapsis pass, taking all measurements obtained at distances to the center of Mars larger than 9,000 kilometers (around 30 to 50 minutes per orbit). The bottom panel of Figure 7 shows the flux sputtered by solar wind protons and alpha particles at each MAVEN apoapsis. The sputtered flux is found to generally be between 2 and 6×10^6 cm^{-2} s^{-1}, consistent with the long-term sputtered flux computed in section 4. At least five enhancements in the computed sputtered flux are seen (i.e., 22 and 26 February, 3-4, 7, and 8-9 March) and last less than 1 to 2 days each. Each of these enhancements occur when solar wind ion fluxes increase as seen in the SWIA energy spectrogram shown by the second panel of Figure 7 and total ion fluxes integrated over energy (third panel of Figure 7). These solar wind ion flux enhancements are correlated with the arrival of very energetic ions observed by MAVEN/SEP.

The time variability in sputtered fluxes reported here is due to ions with energies lower than 20 keV observed by SWIA and STATIC. Fluxes of very energetic ions observed by MAVEN/SEP, even when significantly increased during the March 2015 events, remain low enough to contribute to less than 2% of the total sputtered flux, independent of the assumed composition (protons, alpha particles, or oxygen ions). The maximum to minimum ratio of sputtered flux in the considered time period is of ~50, similar to that reported by Killen et al. (2012) regarding the effect of ICMEs on surface sputtering at the Moon.

6. Summary and Discussion

The MAVEN spacecraft repeatedly crossed the orbit of Phobos from January 2015 to February 2019, observing there only a limited range of MSO longitudes (or solar local time) on each orbit but observing over the mission duration all the MSO longitudes and therefore plasma regions encountered by Phobos several times: the solar wind, magnetosheath, and magnetotail. This orbit, in conjunction with the three MAVEN ion instruments, SWIA, STATIC, and SEP, provide an unprecedented ability to constrain the in situ ion environment that impacts the surface of Phobos (section 2).

The long-term average multispecies ion environment that Phobos is exposed to has been constructed from MAVEN ion measurements from cold plasma energies to several MeV. In this long-term picture, keV to tens of keV planetary pickup oxygen ions, O^+, are found at all solar local times. Furthermore, this study reveals that fluxes of energetic molecular oxygen ions, O_2^+, are of the same order as fluxes of O^+ in the magnetotail, contrary to expectations from numerical models (Curry et al., 2014).

Ions can alter the surface of Phobos in many ways, so that the long-term average ion environment presented in section 3 may be used in the future to understand Phobos regolith properties that will be revealed as of 2025 by the Martian Moons Exploration (MMX) mission (Usui et al., 2018). Poppe et al. (2018) conducted a similar effort at the Moon, using ARTEMIS ion measurements to explain regolith samples gathered by the Apollo missions. Space weathering by solar wind ions has also been shown to be important at asteroid Itokawa from samples returned by the Hayabusa mission (Harries & Langenhorst, 2014; Keller & Berger, 2014; Matsumoto et al., 2015; Noguchi et al., 2014).

The flux of atoms sputtered from the surface of Phobos by the long-term average ion environment has then been assessed. Solar wind protons and alpha particles are found to dominate the sputtering of neutrals over planetary pickup ions in the solar wind and magnetosheath regions. Downstream of Mars, for MSO longitudes between 135° and 210°, MAVEN confirms what has been proposed first by Poppe and Curry (2014) with a model of planetary ions, namely, that atomic oxygen ions, O^+, dominate sputtering over the solar wind. In addition, MAVEN reveals that molecular oxygen ions, O_2^+, sputter surface atoms as much or more than oxygen ions in the tail (section 4).

We therefore confirm that Phobos surface sputtering is linked to the atmospheric escape of Mars. The escape rate and the Interplanetary Magnetic Field that drive planetary ion fluxes that impact Phobos both vary in time. The long-term average ion environment and its sputtering effect shown in this study and based on in situ measurements average together these short time scale variations, which numerical models typically cannot. This study also captures part of the longer time scale solar cycle variation observed during the 4 years of the MAVEN mission. It may therefore be one of the best available estimates of Phobos surface ion sputtering on geological time scales of several billion years. In the early Solar System, planetary ions may have had a more important role in Phobos surface sputtering than today as the atmospheric escape rate was higher by maybe a factor of 7 (Ramstad et al., 2018) and the Martian magnetosphere may have been larger.

Section 5 has shown that the Phobos surface sputtered flux increased by a factor of up to 50 during periods of 1 to 2 days in response to the series of ICMEs that hit the Martian system in March 2015 (e.g., Lee et al., 2017). These enhancements and their durations can clearly be sufficient to significantly increase densities in the putative neutral torus of Phobos. Poppe et al. (2016) presented a numerical model of the Phobos neutral torus assuming a sputtered flux consistent with the long-term value obtained in this study. A modeling effort could be conducted in the future to balance the increase of surface sputtered rate with the likely shortened neutral lifetime against ionization, to determine if and to what extent densities in the neutral torus of Phobos increased in March 2015. In any case, both the increase of surface sputtered rate and ionization rate will result in an increase of the flux of ions created from the putative Phobos neutral torus. Poppe et al. (2016) detail that these ions can be used to unambiguously detect the Phobos neutral torus, and section 5 of this study points out that periods of solar wind activity are conducive to this discovery.

Acknowledgments
MAVEN SEP, SWIA, and STATIC data are publicly available on the NASA Planetary Data System website (https://pds-ppi.igpp.ucla.edu/) in respectively the volumes named "MAVEN-Mars-SEP", "MAVEN-Mars-SWIA", and "MAVEN-Mars-STATIC". Energy fluxes of the long-term average ion environment seen by Phobos, computed in this study and observed by the MAVEN SWIA, STATIC, and SEP instruments, can be accessed at https://figshare.com/articles/DataProducts_LongTerm_Ions_Phobos/10086065. We thank D. Larson (UCB/SSL) for the Tplot software that has been used to produce Figures 2, 3, 4 and 7. Q. Nénon and A. R. Poppe acknowledge funding from the NASA Solar System Research Virtual Institute/DREAM2 Team, grant NNX14AG16A. A. Rahmati, C. O. Lee, J. P. McFadden, and C. M. Fowler acknowledge funding by NASA through MAVEN Project subcontracts managed by LASP, University of Colorado under the direction of the MAVEN Principal Investigator, B.M. Jakosky. The MAVEN mission has been made possible through NASA sponsorship and the dedicated efforts of NASA Goddard Space Flight Center, LASP, Lockheed project management, and the MAVEN Technical and Science Teams.

References

Barabash, S., Dubinin, E., Pissarenko, N., Lundin, R., & Russell, C. T. (1991). Picked-up protons near Mars: Phobos observations. *Geophysical Research Letters*, *18*(10), 1805–1808. https://doi.org/10.1029/91GL02082

Barghouty, A. F., Meyer, F. W., Harris, P. R., & Adams, J. H. Jr. (2011). Solar-wind protons and heavy ions sputtering of lunar surface materials. *Nuclear Instruments and Methods in Physics Research Section B: Beam Interactions with Materials and Atoms*, *269*(11), 1310–1315. https://doi.org/10.1016/j.nimb.2010.12.033

Biersack, J. P., & Eckstein, W. (1984). Sputtering studies with the Monte Carlo Program TRIM.SP. *Applied Physics A*, *34*, 73–94. https://doi.org/10.1007/BF00614759

Christoffersen, R., Keller, L. P., & McKay, D. S. (1996). Microstructure, chemistry, and origin of grain rims on ilmenite from the lunar soil finest fraction. *Meteoritics and Planetary Science*, *31*, 835–848. https://doi.org/10.1111/j.1945-5100.1996.tb02117.x

Cipriani, F., Witasse, O., Leblanc, F., Modolo, R., & Johnson, R. E. (2011). A model of interaction of Phobos' surface with the Martian environment. *Icarus*, *212*(2), 643–648. https://doi.org/10.1016/j.icarus.2011.01.036

Curry, S. M., Liemohn, M., Fang, X., Ma, Y., Slavin, J., Espley, J., et al. (2014). Test particle comparison of heavy atomic and molecular ion distributions at Mars. *Journal of Geophysical Research: Space Physics*, *119*, 2328–2344. https://doi.org/10.1002/2013JA019221

Curry, S. M., Luhmann, J. G., Ma, Y. J., Dong, C. F., Brain, D., Leblanc, F., et al. (2015). Response of Mars O+ pickup ions to the 8 March 2015 ICME: Inferences from MAVEN data-based models. *Geophysical Research Letters*, *42*, 9095–9102. https://doi.org/10.1002/2015GL065304

Dong, C., Ma, Y., Bougher, S. W., Toth, G., Nagy, A. F., Halekas, J. S., et al. (2015). Multifluid MHD study of the solar wind interaction with Mars' upper atmosphere during the 2015 March 8th ICME event. *Geophysical Research Letters*, *42*, 9103–9112. https://doi.org/10.1002/2015GL065944

Dong, Y., Fang, X., Brain, D. A., McFadden, J. P., Halekas, J. S., Connerney, J. E., et al. (2015). Strong plume fluxes at Mars observed by MAVEN: An important planetary ion escape channel. *Geophysical Research Letters*, *42*, 8942–8950. https://doi.org/10.1002/2015GL065346

Dong, Y., Fang, X., Brain, D. A., McFadden, J. P., Halekas, J. S., Connerney, J. E. P., et al. (2017). Seasonal variability of Martian ion escape through the plume and tail from MAVEN observations. *Journal of Geophysical Research: Space Physics*, *122*, 4009–4022. https://doi.org/10.1002/2016JA023517

Dubinin, E., Fränz, M., Woch, J., Roussos, E., Barabash, S., Lundin, R., et al. (2006). Plasma morphology at Mars. ASPERA-3 observations. *Space Science Reviews*, *126*(1-4), 209–238. https://doi.org/10.1007/s11214-006-9039-4

Dubinin, E., Lundin, R., Norberg, O., & Pissarenko, N. (1993). Ion acceleration in the Martian tail: Phobos observations. *Journal of Geophysical Research*, *98*(A3), 3991–3997. https://doi.org/10.1029/92JA02233

Farrell, W. M., Halekas, J. S., Fatemi, S., Poppe, A. R., Hartzell, C., Marshall, J. R., et al. (2018). Anticipated electrical environment at Phobos: Nominal and solar storm conditions. *Advances in Space Research*, *62*(8), 2199–2212. https://doi.org/10.1016/j.asr.2017.08.009

Halekas, J. S., Ruhunusiri, S., Harada, Y., Collinson, G., Mitchell, D. L., Mazelle, C., et al. (2017). Structure, dynamics, and seasonal variability of the Mars-solar wind interaction: MAVEN Solar Wind Ion Analyzer in-flight performance and science results. *Journal of Geophysical Research: Space Physics*, *122*, 547–578. https://doi.org/10.1002/2016JA023167

Halekas, J. S., Taylor, E. R., Dalton, G., Johnson, G., Curtis, D. W., McFadden, J. P., et al. (2015). The solar wind ion analyzer for MAVEN. *Space Science Reviews*, *195*(1-4), 125–151. https://doi.org/10.1007/s11214-013-0029-z

Harries, D., & Langenhorst, F. (2014). The mineralogy and space weathering of a regolith grain from 25143 Itokawa and the possibility of annealed solar wind damage. *Earth, Planets and Space*, *66*(1), 163. https://doi.org/10.1186/s40623-014-0163-1

Inui, S., Seki, K., Namekawa, T., Sakai, S., Brain, D. A., Hara, T., et al. (2018). Cold dense ion outflow observed in the Martian-induced magnetotail by MAVEN. *Geophysical Research Letters*, *45*, 5283–5289. https://doi.org/10.1029/2018GL077584

Inui, S., Seki, K., Sakai, S., Brain, D. A., Hara, T., McFadden, J. P., et al. (2019). Statistical study of heavy ion outflows from Mars observed in the Martian induced magnetotail by MAVEN. *Journal of Geophysical Research: Space Physics*, *124*, 5482–5497. https://doi.org/10.1029/2018JA026452

Jakosky, B. M., Grebowsky, J. M., Luhmann, J. G., & Brain, D. A. (2015). Initial results from the MAVEN mission to Mars. *Geophysical Research Letters*, *42*, 8791–8802. https://doi.org/10.1002/2015GL065271

Jakosky, B. M., Grebowsky, J. M., Luhmann, J. G., Connerney, J., Eparvier, F., Ergun, R., et al. (2015). MAVEN observations of the response of Mars to an interplanetary coronal mass ejection. *Science*, *350*(6261). https://doi.org/10.1126/science.aad0210

Keller, L. P., & Berger, E. L. (2014). A transmission electron microscope study of Itokawa regolith grains. *Earth, Planets and Space*, *66*(1), 71. https://doi.org/10.1186/1880-5981-66-71

Keller, L. P., & McKay, D. S. (1997). The nature and origin of rims on lunar soil grains, *Geochem*. *Geochimica et Cosmochimica Acta*, *61*(11), 2331–2341. https://doi.org/10.1016/S0016-7037(97)00085-9

Killen, R. M., Hurley, D. M., & Farrell, W. M. (2012). The effect on the lunar exosphere of a coronal mass ejection passage. *Journal of Geophysical Research*, *117*, E00K02. https://doi.org/10.1029/2011JE004011

Larson, D. E., Lillis, R. J., Lee, C. O., Dunn, P. A., Hatch, K., Robinson, M., et al. (2015). The MAVEN solar energetic particle investigation. *Space Science Reviews*, *195*(1-4), 153–172. https://doi.org/10.1007/s11214-015-0218-z

Lee, C. O., Hara, T., Halekas, J. S., Thiemann, E., Chamberlin, P., Eparvier, F., et al. (2017). MAVEN observations of the solar cycle 24 space weather conditions at Mars. *Journal of Geophysical Research: Space Physics*, *122*, 2768–2794. https://doi.org/10.1002/2016JA023495

Liemohn, M. W., & Xu, S. (2018). Recent advances regarding the Mars magnetotail current sheet. Chapter 11. In *Electric Currents in Geospace and Beyond, Geophysical Monograph 235* (pp. 177–190). Wiley. https://doi.org/10.1002/9781119324522.ch11

Lundin, R., Barabash, S., Holmström, M., Nilsson, H., Futaana, Y., Ramstad, R., et al. (2013). Solar cycle effects on the ion escape from Mars. *Geophysical Research Letters*, *40*, 6028–6032. https://doi.org/10.1002/2013GL058154

Matsumoto, T., Tsuchiyama, A., Miyake, A., Noguchi, T., Nakamura, M., Uesugi, K., & Nakano, T. (2015). Surface and internal structures of a space-weathered rim of an Itokawa regolith particle. *Icarus*, *257*, 230–238. https://doi.org/10.1016/j.icarus.2015.05.001

Matsunami, N., Yamamura, Y., Itikawa, Y., Itoh, N., Kazumata, Y., Miyagawa, S., et al. (1984). Energy dependence of the ion-induced sputtering yields of monatomic solids. *Atomic data and nuclear data tables*, *31*(1), 1–80. https://doi.org/10.1006/adnd.1996.0005

McFadden, J. P., Kortmann, O., Curtis, D., Dalton, G., Johnson, G., Abiad, R., et al. (2015). MAVEN Suprathermal and Thermal Ion Composition (STATIC) instrument. *Space Science Reviews*, *195*(1-4), 199–256. https://doi.org/10.1007/s11214-015-0175-6

Modolo, R., Chanteur, G. M., Dubinin, E., & Matthews, A. P. (2005). Influence of the solar EUV flux on the Martian plasma environment. In *Annales Geophysicae* (Vol. 23, pp. 433–444). Copernicus Gmbh. https://doi.org/10.5194/angeo-23-433-2005

Mutzke, A., Schneider, R., Eckstein, W., Dohmen, R., Schmid, K., Toussaint, U. V., & Badelow, G. (2019). SDTrimSP Version 6.00.

Nagy, A., Winterhalter, D., Sauer, K., Cravens, T. E., Brecht, S., azelle, C., et al. (2004). The plasma environment of Mars. *Space Science Reviews*, *111*, 33–114. https://doi.org/10.1023/B:SPAC.0000032718.47512.92

Noguchi, T., Kimura, M., Hashimoto, T., Konno, M., Nakamura, T., Zolensky, M. E., & Ogami, T. (2014). Space weathered rims found on the surfaces of the Itokawa dust particles. *Meteoritics & Planetary Science*, *49*(2), 188–214. https://doi.org/10.1111/maps.12111

Pieters, C. M., Murchie, S., Thomas, N., & Britt, D. (2014). Composition of Surface Materials on the Moons of Mars. *Planetary and Space Science*, *102*, 144–151. https://doi.org/10.1016/j.pss.2014.02.008

Poppe, A. R., & Curry, S. M. (2014). Martian planetary heavy ion sputtering of Phobos. *Geophysical Research Letters*, *41*, 6335–6341. https://doi.org/10.1002/2014GL061100

Poppe, A. R., Curry, S. M., & Fatemi, S. (2016). The Phobos neutral and ionized torus. *Journal of Geophysical Research: Planets*, *121*, 770–783. https://doi.org/10.1002/2015JE004948

Poppe, A. R., Farrell, W. M., & Halekas, J. S. (2018). Formation timescales of amorphous rims on lunar grains derived from ARTEMIS observations. *Journal of Geophysical Research: Planets*, *123*, 37–46. https://doi.org/10.1002/2017JE005426

Rahmati, A., Larson, D. E., Cravens, T. E., Lillis, R. J., Dunn, P. A., Halekas, J. S., et al. (2015). MAVEN insights into oxygen pickup ions at Mars. *Geophysical Research Letters*, *42*, 8870–8876. https://doi.org/10.1002/2015GL065262

Rahmati, A., Larson, D. E., Cravens, T. E., Lillis, R. J., Halekas, J. S., McFadden, J. P., et al. (2017). MAVEN measured oxygen and hydrogen pickup ions: Probing the Martian exosphere and neutral escape. *Journal of Geophysical Research: Space Physics*, *122*, 3689–3706. https://doi.org/10.1002/2016JA023371

Rahmati, A., Larson, D. E., Cravens, T. E., Lillis, R. J., Halekas, J. S., McFadden, J. P., et al. (2018). Seasonal variability of neutral escape from Mars as derived from MAVEN pickup ion observations. *Journal of Geophysical Research: Planets*, *123*, 1192–1202. https://doi.org/10.1029/2018JE005560

Ramstad, R., Barabash, S., Futaana, Y., Nilsson, H., & Holmström, M. (2017). Global Mars-solar wind coupling and ion escape. *Journal of Geophysical Research: Space Physics*, *122*, 8051–8062. https://doi.org/10.1002/2017JA024306

Ramstad, R., Barabash, S., Futaana, Y., Nilsson, H., & Holmström, M. (2018). Ion escape from mars through time: An extrapolation of atmospheric loss based on 10 years of Mars Express measurements. *Journal of Geophysical Research: Planets*, *123*, 3051–3060. https://doi.org/10.1029/2018JE005727

Schaible, M. J., Dukes, C. A., Hutcherson, A. C., Lee, P., Collier, M. R., & Johnson, R. E. (2017). Solar wind sputtering rates of small bodies and ion mass spectrometry detection of secondary ions. *Journal of Geophysical Research: Planets*, *122*, 1968–1983. https://doi.org/10.1002/2017JE005359

Steinbrüchel, C. (1985). On the sputtering yield of molecular ions. *Journal of Vacuum Science & Technology A: Vacuum, Surfaces, and Films*, *3*(5), 1913–1915. https://doi.org/10.1116/1.572944

Szabo, P. S., Chiba, R., Biber, H., Stadlmayr, R., Berger, B. M., Mayer, D., & Fleig, J. (2018). Solar wind sputtering of wollastonite as a lunar analogue material—Comparisons between experiments and simulations. *Icarus*, *314*, 98–105. https://doi.org/10.1016/j.icarus.2018.05.028

Trotignon, J. G., Mazelle, C., Bertucci, C., & Acuña, M. H. (2006). Martian shock and magnetic pile-up boundary positions and shapes determined from the Phobos 2 and Mars Global Surveyor data sets. *Planetary and Space Science*, *54*(4), 357–369. https://doi.org/10.1016/j.pss.2006.01.003

Usui, T., Kuramoto, K., & Kawakatsu, Y. (2018). Martian Moons eXploration (MMX): Japanese Phobos Sample Return Mission. In 42nd COSPAR Scientific Assembly (Vol. 42).

Verigin, M. I., Shutte, N. M., Galeev, A. A., Gringauz, K. I., Kotova, G. A., Remizov, A. P., et al. (1991). Ions of planetary origin in the Martian magnetosphere (Phobos 2/TAUS experiment). *Planetary and Space Science*, *39*(1-2), 131–137. https://doi.org/10.1016/0032-0633(91)90135-W

Yamauchi, M., Futaana, Y., Fedorov, A., Frahm, R. A., Winningham, J. D., Dubinin, E., et al. (2011). Comparison of accelerated ion populations observed upstream of the bow shocks at Venus and Mars. In *Annales Geophysicae* (Vol. *29*, pp. 511–528). Copernicus GmbH. https://doi.org/10.5194/angeo-29-511-2011

Ziegler, J., Biersack, J., & Ziegler, M. (2008). *SRIM, the stopping and range of ions in matter*. Chester, MD: SRIM Company.

Erratum

In the originally published version of this article, several instances of text were incorrectly typeset. The following have since been corrected and this version may be considered the authoritative version of record.

The formatting of Equation 1 was corrected.

In section 5, a typographical error was fixed.

In section 6, “Itakawa” was corrected to “Itokawa”.